Fatigue Behavior and Life Prediction of PI/SiO_2 Nanocomposite Films

Z. D. Wang, X. X. Zhao

Institute of Mechanics, School of Civil Engineering, Beijing JiaoTong University, Beijing 100044, China

Received 9 August 2008; accepted 15 October 2008
DOI 10.1002/app.29767
Published online 4 March 2009 in Wiley InterScience (www.interscience.wiley.com).

ABSTRACT: In this report, the fatigue behavior and lifetime of Polyimide/silica (PI/SiO_2) hybrid films are investigated. To evaluate the fatigue property of this class of hybrid films, the stress-life cyclic experiments under tension–tension fatigue loading with 10 Hz of the frequency are performed, and the stress ratio is 0.1. Dynamic creep and cyclic softening/hardening are analyzed based on the change of hysteresis loops during the fatigue process. The structure-property relations are discussed to further understand their phenomenon and deformation mechanisms. To predict the fatigue life of this class of hybrid films, a semi-empirical model is proposed based on fatigue modulus concept. The simulated results are well agreeable with the testing values. © 2009 Wiley Periodicals, Inc. J Appl Polym Sci 112: 3276–3283, 2009

Key words: thin film; hysteresis loop; viscoelastic behavior; fatigue modulus

INTRODUCTION

Fatigue properties are critical for materials working under cyclic loads. It is known that the fatigue failure of polymers and matrix-dominated polymeric composites is more complicated than that of the well-studied metals due to the viscoelastic response and the large plastic deformation capability of materials. Earlier researches focused on the experiments and theoretical analyses of the fatigue properties of various polymers,[1–3] and more recently, there were more research reports about polymeric-matrix composites.[4–7]

In view of the fact that, using nanomaterials as fillers is becoming the state-of-the-art technology in materials science; numerous works have been done and many improved mechanical properties have been achieved with incorporations of nanofillers into polymeric matrices in the past years.[8–12] However, the studies until now are focused on quasi-static mechanical properties of this class of composite materials, e.g., how to improve their strength, stiffness, and toughness by adding small number of nanoinorganic fillers into polymeric matrices. The fatigue properties are hardly reported. As considering their long-time service, especially under alternative loading conditions, essential information about the fatigue property seems to be necessary.

This article reports some results of the fatigue deformation of PI/SiO_2 hybrid films doped with silica nanoinorganic fillers. The silica doping levels used in the experiments are varied by weight in the range of 0–8%. The hysteresis loop method is used to determine the strain amplitude and mean strain in every fatigue cycle, which are mainly associated with the cyclic softening/hardening and dynamic creep of materials, respectively. The structure-property relationship is also analyzed to have a better understanding of the fatigue properties of this class of composite films. Finally, a prediction model about the fatigue life is proposed by using residual modulus degradation concept.

EXPERIMENTAL

Materials

As an important insulating material, Polyimide (PI) films own some exclusive properties, such as outstanding thermal stability, excellent mechanical and electrical properties. To further decrease the coefficient of thermal expansion (CTE) to be comparable with that of metallic substrates and improve mechanical properties as well (e.g., low-temperature toughness and high-temperature strength), different inorganic nanofillers have been considered to synthesize PI/nanoinorganic composite films.[13–15] Among them, commercial available silica is an ideal candidate

Correspondence to: Z. D. Wang (zhdwang@bjtu.edu.cn).
Contract grant sponsor: Natural Science Foundation of China; contract grant numbers: 10502005, 10872025.
Contract grant sponsor: Ministry of Education of the People's Republic of China (NECT).

and has attracted a broad interest because of its low CTE, low cost, and matured synthesizing technique (sol–gel method). However, the mechanical properties of PI/SiO_2 hybrid films synthesized by the traditional sol–gel method will decrease quickly at higher silica doping levels due to the increased particle size. To overcome this issue, an improved sol–gel process has been introduced, as shown in Ref. 16, to homogenously disperse silica particles into PI matrix and keep them under nanosize at higher silica doping levels. The synthesizing process can be simply described as the following.

Some commercial available materials are used, namely, pyromellitic dianhydride (PMDA, $C_{10}H_2O_6$) and oxydianiline diamine (ODA, $C_{12}H_{12}N_2O$) from Tecnid Enterprise Co. (Beijing, China), tetraethoxysilane (TEOS), ethanol (EtOH), and catalyst from Beijing Chemical Co. (Beijing, China), *N*,*N*-dimethylacetamide (DMAc, [$(CH_3)_2NCOCH_3$)]) is desiccated by molecular sieve before use. ODA is first dissolved in DMAc under a nitrogen atmosphere. TEOS, EtOH, and catalyst are then added to form the solution. After stirring for about 30 min, PMDA are added and subsequently stirred for about 6 h to produce a homogeneous solution. Hybrid films are obtained through the same thermal treatment as above. Finally, four types of thin films, such as pure PI, PI/SiO_2 hybrid films with 1, 3, and 8 wt % silica doping levels, are synthesized and prepared for the following experiment.

Measurements

The prepared films with a thickness of $\sim$ 0.035 mm are cut into the specimens with 4 mm in width and 35 mm in length. The gauge length is 20 mm. All tests are performed in an INSTRON digital microelectromagnetism testing system with a dynamic capacity of 10 N, maximum displacement of 2.5 mm, and maximum frequency of 50 Hz. A sinusoidal force oscillation at 10 Hz with stress ratio $R = 0.1$ (minimum stress divided by maximum stress) is applied. The stress is received based on the applied load divided by the cross-sectional area of specimens, and the strain values are recorded by an extensometer. The two fixing sides of the extensometer are, respectively, connected with the upper and lower jigs of the testing system. The microdeformation of the jigs between the two fixing sides of the extensometer is neglected. The experimental temperature and ambient humidity were 298 K and 45%, respectively.

RESULTS AND DISCUSSION

Cyclic softening/hardening and dynamic creep

Before carrying the practical stress-controlled cyclic experiments, the maximum and minimum stresses in every cycle are firstly examined to ensure that the experimental results are reliable. It shows that the real stress-amplitude does not reach to the presetting value at the first few seconds, which might be due to the restriction of the loading system of the testing machine. Therefore, the experimental data at the first few seconds are neglected in the following discussion.

Figure 1 presents some typical hysteresis loops of pure PI and PI/SiO_2 hybrid films in different fatigue stages. The values of the normalized-fatigue cycles (cyclic number N divided by the fatigue life of materials N_f) for different hysteresis loops are listed and the corresponding parts of stress–strain curves under quasi-static tensile load are also shown in Figure 1 for a comparison. The results exhibit that the energy loss (the area enclosed in hysteresis loops) and the strain amplitude are significantly reduced with increasing the silica doping levels, which indicates that the presence of silica-fillers can effectively decrease the viscosity and improve the deformation stiffness of PI matrix. In addition, the dynamic deformation resistances of pure PI and PI/SiO_2 hybrid films are much higher than the quasi-static values, which might be due to the viscoelastic response of materials.

The development of hysteresis loops can also provide the information about cyclic softening/hardening and dynamic creep of materials. To evaluate the cyclic softening/hardening and dynamic creep of this class of hybrid films, two parameters, strain amplitude ε_a and mean strain ε_m, are defined as follows:

$$\varepsilon_a = \varepsilon_{\max} - \varepsilon_{\min}, \tag{1}$$

$$\varepsilon_m = \frac{1}{2}(\varepsilon_{\max} + \varepsilon_{\min}), \tag{2}$$

where, $\varepsilon_{\max}$ and $\varepsilon_{\min}$ denote the maximum and minimum strains in hysteresis loops, respectively. ε_a is constant when there is no cyclic softening/hardening phenomenon and ε_m will not change if there is no dynamic creep during the fatigue process. Hence, the values of ε_a and ε_m are greatly determined by the cyclic softening/hardening and the dynamic creep of materials, respectively.

The experimental results of the strain amplitude ε_a and the mean strain ε_m about pure PI and PI/SiO_2 hybrid thin films subjected to fatigue loading are shown in Figure 2. The stress amplitudes can be referred in Figure 1. The results in Figure 2 exhibit that the strain amplitude is decreased and the mean strain is increased during the fatigue process, which reflects the phenomena of cyclic hardening and dynamic creep. The more remarkable cyclic hardening of pure PI than that of other hybrid films confirms that it is not caused by the presence of silica-fillers. In addition, cyclic hardening and dynamic

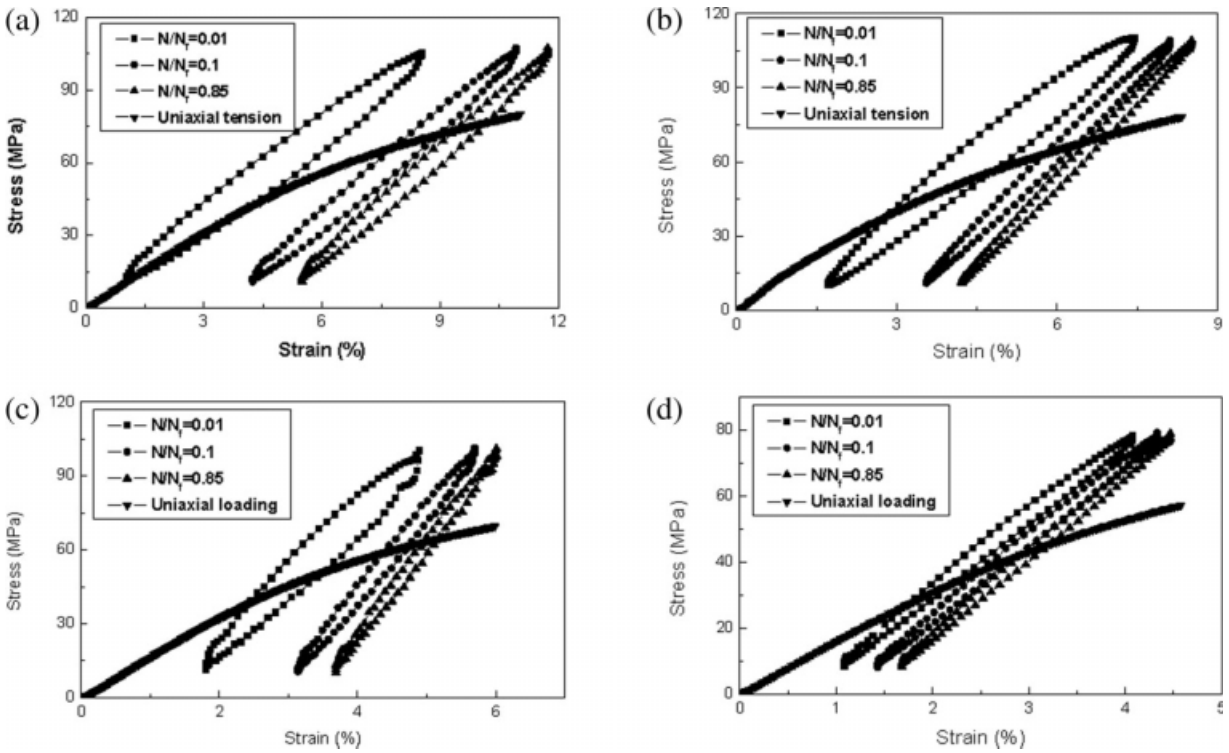

Figure 1 Typical uniaxial-loading and fatigue tension-tension curves of pure PI and PI/SiO_2 hybrid films. (a) Pure PI; (b) Films with 1 wt % SiO_2; (c) Films with 3 wt % SiO_2; (d) Films with 8 wt % SiO_2.

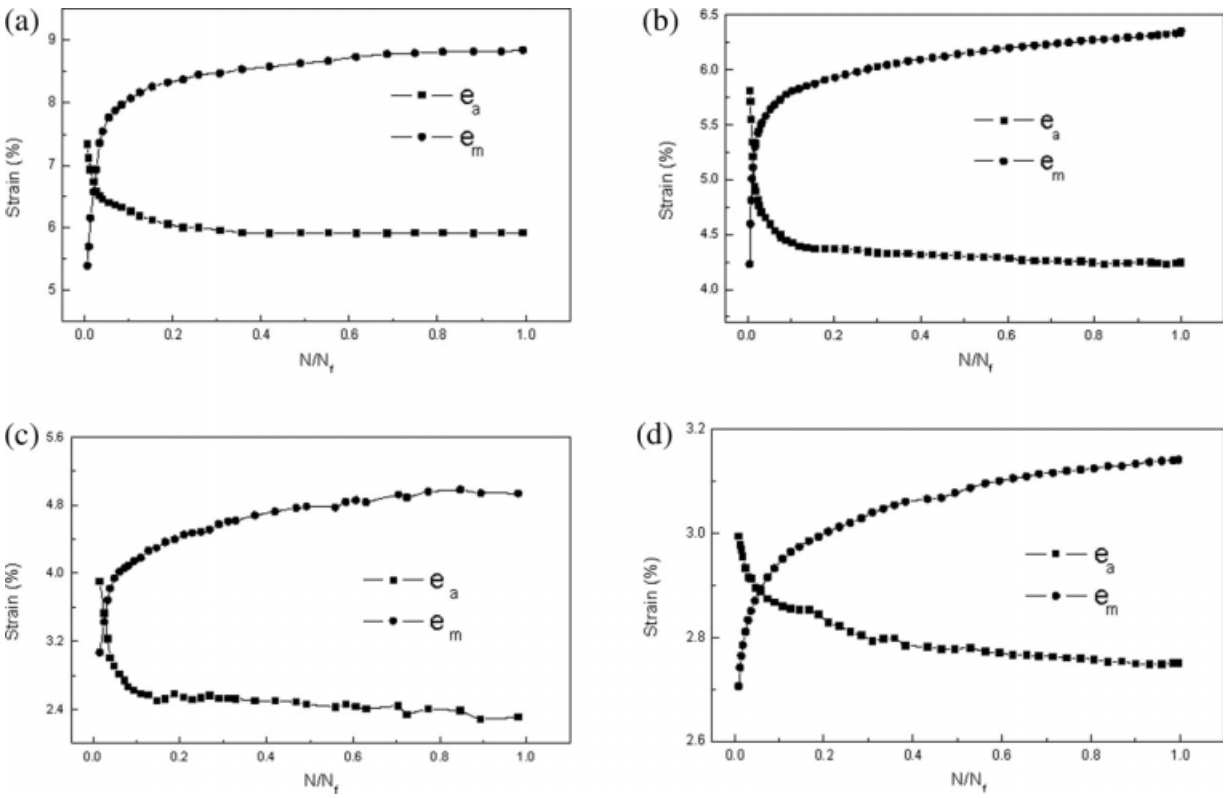

Figure 2 Curves of strain amplitude and mean strain vs. normalized fatigue cycles for pure PI and PI/SiO_2 hybrid films. (a) Pure PI; (b) Films with 1 wt % SiO_2; (c) Films with 3 wt % SiO_2; (d) Films with 8 wt % SiO_2.

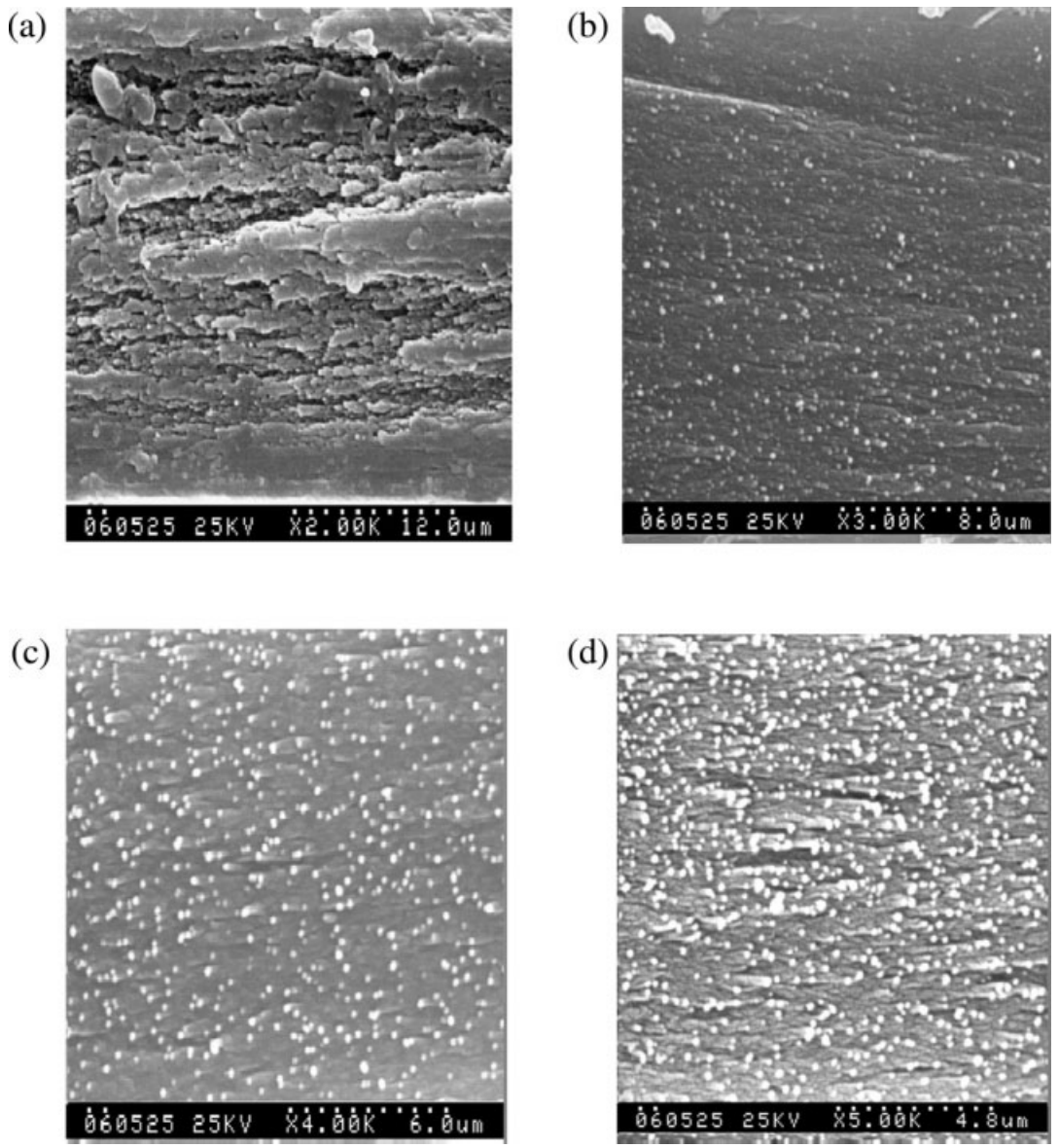

Figure 3 SEM micrographs of pure PI and PI/SiO_2 hybrid thin films under fatigue conditions.

creep of pure PI are especially significant in the primary fatigue stage with the normalized fatigue cycles lower than 0.2, and then a steady fatigue stage is followed. As the silica content increases to 8 wt %, there is no obvious transition observed from primary to secondary fatigue stage. The presence of silica-fillers significantly decelerates the cyclic hardening and dynamic creep.

Structure-property relations

Figure 3 provides SEM micrographs of fatigue fracture surfaces about pure PI and PI/SiO_2 hybrid thin films. The loading direction is perpendicular to the

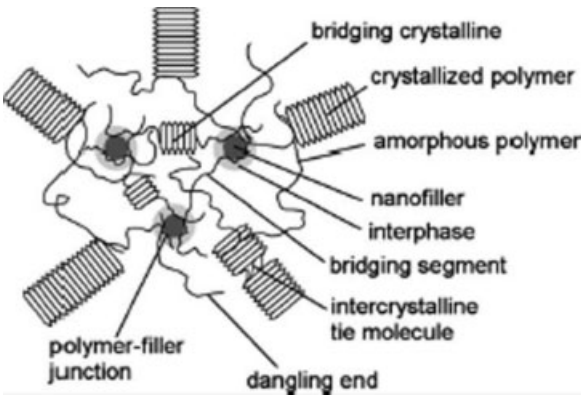

Figure 4 Schematically representative structure of nanofiller–semicrystalline polymer composites.

fracture surface. According to Figure 3, multiscale-like fatigue striations can be observed in the fracture surface of pure PI film, and many microcracks exist in PI/SiO_2 composite films. Moreover, the SEM micrographs confirm that silica-fillers are homogeneously dispersed into PI matrix. Most particles are 50 to 120 nm in diameter, and a few aggregated particles are larger than 150 nm in diameter.

To give a structure-property analysis, Figure 4 presents a representative configuration of the nanoparticles/polymer composites schematically. Crystallized chains, amorphous regions, polymer-filler junction, intercrystalline tie molecule, segment, and crystalline bridging are considered carefully. Similar to other semicrystalline polymers, PI can be primarily regarded as the composition of crystallized chains and amorphous regions in the view of microstructure. The response of crystallized chains to external load is instantaneous and elastic, whereas the response of the amorphous region is time-dependent and viscoelastic. Since the crystallized chains are comparatively fixed and the amorphous regions are variable, the additive of nanosilica particles will mainly exist in the amorphous regions as shown in Figure 4.

The dynamic creep and cyclic hardening of viscoelastic materials are associated with different deformation mechanisms. In the primary fatigue stage, the dynamic creep is associated with the large-scale viscous flow of amorphous regions, but the cyclic hardening is primarily caused by the orientated strain hardening of crystallized chains. During this stage, the dynamic creep and cyclic hardening are remarkable due to the lack of the effective limitation. However, as time goes on, both viscous flow of amorphous regions and orientated hardening of crystallized-chains become more difficult along the loading direction, and the secondary steady fatigue deformation is followed. In the secondary fatigue stage, the dynamic creep is commonly due to the damage of crystallized and amorphous chains, and the cyclic hardening might be associated with the cyclic plastic deformation of crystallized and amorphous chains.

According to the results shown in Figure 2, the influence of nanofillers on the dynamic creep and cyclic hardening seems to be remarkable. Commonly speaking, the amount of small particles in unit volume matrix is higher than that of the large ones by several orders of magnitude, and these small particles with bridging segments can form a much huge and dense network.[17] The network structure of nanofillers can effectively restrict the viscous flow in amorphous regions and enhance the capability to bear loads. Hence, the viscous dissipation in hysteresis loops is significantly decreased and the deformation resistance is also improved with increasing the silica doping levels. Moreover, the network structure of nanofillers might have the function to retard the viscous flow in amorphous regions and decelerate the orientated deformation of crystallized chains. Therefore, the secondary steady deformation stage of PI/SiO_2 hybrid films is more significant than that of pure PI film. As the silica doping level is increased to 8 wt %, no remarkable transition from primary to secondary fatigue stage is observed (Fig. 2).

FATIGUE LIFE PREDICTION

The fatigue property is critical for materials to meet the request of long-time applications, especially under alternative loading conditions. Experiments can only provide fatigue properties of materials at limited stress levels. To determine the fatigue life of materials on any condition, an effective theoretical model must be received. Basically, the fatigue life prediction model can be divided into three classes as follows: residual strength degradation models,[18,19] residual stiffness degradation models,[20,21] and fatigue energy accumulation models.[22,23] The main obstacle of the residual strength degradation models is that they cannot realize nondestructive monitoring, and that of fatigue energy accumulation models is that it is difficult to effectively differentiate the energy causing fatigue failure of materials from that dissipated due to conduction, convection, and radiation during the fatigue process. Comparatively, the residual stiffness degradation models are more popular because they can realize a nondestructive test and the degradation of stiffness parameters is easy to be measured during the fatigue process.

The expressions of residual stiffness degradation models are different when different stiffness parameters (fatigue modulus, elastic modulus, and secant

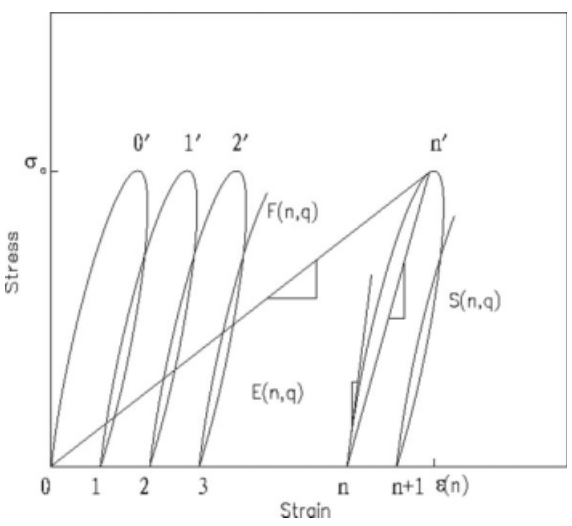

Figure 5 Schematic explanation of fatigue stiffness parameters.

modulus) are considered. The schematic explanation of fatigue modulus, $F(n,q)$, elastic modulus, $E(n,q)$, and secant modulus, $S(n,q)$, under fatigue loads are shown in Figure 5, where, n and q, respectively, denote the cyclic number and normalized applied stress level (the ratio of the maximum fatigue stress and the ultimate tensile strength of materials, σ_u).

Table I lists the experimental results about fatigue life of PI/SiO_2 hybrid thin films with 8 wt % silica doping level at different stress levels. The definition of the modified stress level Q in Table I will be explained later. In the following section, a new fatigue life prediction model will be proposed, and the comparison is given among the new model and some existed.

New fatigue modulus model

Considering the nonlinear stress–strain response for most polymers and their matrix-dominated composites, Lee and Hwang[24] ever proposed a fatigue stiffness degradation model to predict the fatigue life of matrix-dominated polymer composite laminates as follows:

$$N_f = H\left[P - \frac{\xi}{\sigma_u}\ln\left(\frac{\xi}{\xi - \sigma_u q}\right)\right]^J, \tag{3}$$

where, ξ, H, J, and P are material constants. ξ is determined from static test, P from static and fatigue data, H and J from fatigue data.

According to eq. (3), when the fatigue life $N_f \to \infty$, it results $q \to 0$, which is not correct for most materials. Hence, eq. (3) cannot accurately predict the fatigue life of materials at small stress levels. Here, an improved fatigue life prediction model is proposed. The effect of asymmetrical loading is considered as well.

TABLE I
Stress Level and Fatigue Life of PI/SiO_2 with 8 wt % Silica Doping Level

Specimen	Stress level (q)	Modified stress level (Q)	Fatigue life (N_f)
No.1	0.8169	0.6675	6281
No.2			10549
No.3			10666
No.4	0.7901	0.6288	22181
No.5			10871
No.6			12199
No.7	0.6975	0.5092	21997
No.8			23907
No.9			32355
No.10	0.6372	0.4415	62361
No.11			71552
No.12			55551
No.13	0.5948	0.3978	317165
No.14			270874
No.15			357816

Due to the nonlinear stress/strain response of most polymers or matrix-dominated polymer composites under uniaxial tension, an exponential model was ever suggested as follows[24,25]:

$$\sigma = \xi[1 - \exp(-r\varepsilon)], \tag{4}$$

where, r is a dimensionless material constant determined from the quasi-static test data using a regression analysis. Material constant ξ has been defined in eq. (3).

The fatigue modulus degradation rate at any fatigue cycle can be assumed to be an exponent function of the fatigue number n, so that

$$\frac{dF(n,q)}{dn} = -cF_0 a e^{-cn}, \tag{5}$$

where, a and c are material constants. F_0 denotes the initial fatigue modulus at the zeroth (or first) cycle, which can be expressed by Young's modulus, E_0, as follows:

$$F_0 = G(q)E_0. \tag{6}$$

Based on the static stress–strain relationship as shown in eq. (4), $G(q)$ can be expressed as follows:

$$G(q) = \frac{\sigma_u q}{\xi \ln\left(\frac{\xi}{\xi - \sigma_u q}\right)}. \tag{7}$$

To predict the fatigue life of materials at a constant stress level, integrating eq. (5) from n_1 to n_2 cycles, the equation yields as follows:

$$F(n_2,q) - F(n_1,q) = F_0 a(e^{-cn_2} - e^{-cn_1}). \tag{8}$$

Substitution of $n_2 = N$, $n_1 = 0$ and initial condition eq. (6) in eq. (8) gives as follows:

$$F(n,q) - F(0,q) = F_0 a(e^{-cN} - 1) = G(q)E_0 a(e^{-cN} - 1). \tag{9}$$

At failure, where $N = N_f$, the above equation becomes the following:

$$F_f = G(q)E_0(ae^{-cN_f} - a + 1). \tag{10}$$

Based on the stiffness degradation concept, the residual stiffness F_f at failure should reach to a constant value as the normalized stress level q is known. Hence,

$$F_f = E_0 q/P, \tag{11}$$

where material constant P has been defined as in eq. (3).

By substituting eq. (11) in eq. (10), it derives as follows:

$$q = PG(q)(ae^{-cN_f} - a + 1). \tag{12}$$

Based on eq. (12), the fatigue failure only happens on the condition of $q \geq PG(q)(1-a)$. Hence, $q = PG(q)(1-a)$ is the minimum normalized stress level leading to the fatigue failure of materials.

Equation (12) can also be expressed as follows:

$$N_f = -\frac{1}{c}\ln\left[\frac{q}{aPG(q)} - \frac{1}{a} + 1\right]. \tag{13}$$

By substituting eq. (7) into eq. (13), the final expression for the fatigue life N_f is derived as follows:

$$N_f = -H\ln\left[\frac{\xi\ln\frac{\xi}{\xi-\sigma_u q}}{aP\sigma_u} - \frac{1}{a} + 1\right], \tag{14}$$

where material constant $H = 1/c$.

Comparing eq. (14) [or eq. (13)] with eq. (3), the significant improvement is that the fatigue stress limit is considered in the new model and expressed as $q = PG(q)(1-a)$.

Of course, since the linear stress/strain relationship is satisfied for most fiber-dominated composites ($G(q)=1$), eq. (14) can be simplified as follows:

$$N_f = -H\ln\left[\frac{q}{aP} - \frac{1}{a} + 1\right]. \tag{15}$$

Modified normalized stress level

For fatigue experiment under sinusoidal load, the normalized stress level q only denotes the ratio of the maximum fatigue stress and the quasi-static failure strength of materials. In fact, in addition to the normalized stress level q, the fatigue property or fatigue life of materials is also sensitive to the waveform of the fatigue load, which is expressed by the stress ratio R.

$$R = \frac{\sigma_{\min}}{\sigma_{\max}}. \tag{16}$$

In eq. (16), $R = -1$ denotes the basic case of fully reversed tension-compression fatigue loading. In this study, the stress ratio R equals to 0.1 (tension–tension fatigue loading). However, the effect of asymmetrical loading is not embodied in eq. (14) and is also not considered in most reported models.

To incorporate the sensitivity of material fatigue life to the fatigue loading mode, Kawai[26] ever proposed a modified stress level Q to replace q, and defined as follows:

$$Q = \frac{\sigma_a}{\sigma_u - \sigma_m} \tag{17}$$

where, σ_a and σ_m represent the stress range and mean stress, respectively, and are expressed as follows:

$$\sigma_a = \frac{1}{2}(1-R)\sigma_{\max}, \tag{18}$$

$$\sigma_m = \frac{1}{2}(1+R)\sigma_{\max}. \tag{19}$$

TABLE II
Static Properties and Material Constants

Elongation at break	Strength (σ_u)	ξ	r
7.88%	89.61 (MPa)	96.63 ± 0.087 (MPa)	32.86 ± 0.07

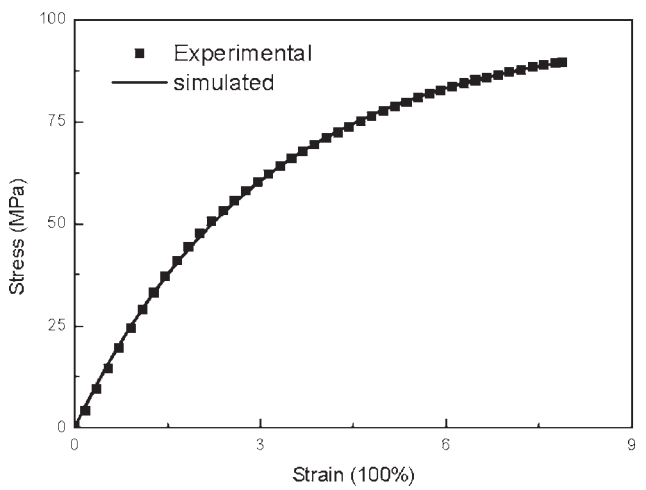

Figure 6 Simulated and experimental results of quasi-static stress-strain relationship of PI/SiO_2 with 8 wt. % silica doping level.

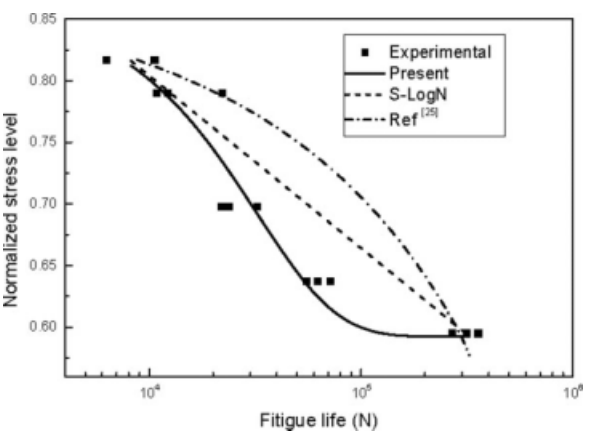

Figure 7 Experimental results and fatigue life predictions of different models.

TABLE III
Estimation of Material Constants

Proposed			S-log N relationship		Ref. 25		
q_0	K	P	K	d	P	H	J
0.590	0.291	0.99997	−0.063	1.366	1.885	273690	3.355

By substituting eq. (18) and eq. (19) into eq. (17), Q can be expressed as follows:

$$Q = \frac{\frac{1}{2}(1-R)q}{1-\frac{1}{2}(1+R)q}. \quad (20)$$

The modified normalized stress level Q can be verified by two special cases. For fully reversed tension-compression fatigue loading ($R = -1$), $Q|_{R=-1} = q$. For quasi-static tension, $Q|_{\sigma_a \to 0, \sigma_m \to \sigma_u} = 1$. Hence, the effect of asymmetrical loading is considered by using Q instead of q in eq. (14) and the testing results with different stress ratios can be comparable. Table I lists q-values and the corresponding Q-values for PI/SiO$_2$ hybrid films with 8 wt % silica doping level.

Experimental verification

Figure 6 presents the quasi-static stress–strain relationship of PI/SiO$_2$ with 8 wt % silica doping level. A highly nonlinear stress–strain response can be found for materials. The regressing result based on eq. (4) is shown in Figure 6 as the solid line, and the material constants are listed in Table II. The result in Figure 6 indicates that the two-parameter exponential model expressed in eq. (4) can effectively regress the experimental data.

Based on the fatigue experimental data of PI/SiO$_2$ films with 8 wt % silica doping level listed in Tables I and II, the experimental and simulated results are shown in Figure 7. To give a comparison, the simulating curves made in Ref. 24 and the conventional linear S-logN relationships are also provided. Table III lists the regressing results of material constants. According to the results shown in Figure 7, it is clear that the simulated result by present model is far better than the other two models. The significant advantage of the new model is that it can capture the fatigue behavior of materials under different normalized stress levels, especially at sufficient higher fatigue cycles, where the normalized stress level will asymptotically reach to a constant value. According to the results listed in Table III, the stress limit q_0 for PI/SiO$_2$ hybrid films with 8 wt % silica doping level is about 0.590, which corresponds to $Q_0 = 0.393$.

CONCLUSIONS

The fatigue properties of PI/SiO$_2$ nanohybrid films with different silica doping levels are experimentally investigated. Significant cyclic hardening and dynamic creep are observed in this class of hybrid films at the beginning fatigue stage, and then decrease quickly. The presence of silica-fillers is effective in improving the deformation resistance and decreasing the viscous dissipation of PI/SiO$_2$ hybrid films under fatigue loads. Moreover, cyclic hardening and dynamic creep in the primary fatigue stage can be decelerated with increasing silica doping levels. SEM micrographs indicate that the silica particles are well-dispersed into PI-matrix under the nanosize for all specimens studied here. The structure-property analysis is used to give an explanation about the phenomena and deformation mechanisms as well.

For fatigue life prediction, a new model is proposed based on the fatigue modulus concept, initial and final conditions. The new model can determine the fatigue stress limit and provide a possibility to predict the fatigue life of materials with different loading waveforms. The simulated results exhibit to be well agreeable with the experimental values.

The authors are indebted to Professor Fu Shao-yun and Mrs. Li Yan for their helps in providing specimens.

References

1. Manson, J. A.; Hertzberg, R. W. Crit Rev Macromol Sci 1973, 1, 433.
2. Rabinowitz, S.; Beardmore, P. J. J Mater Res 1974, 9, 81.
3. Saure, J. A.; Richardson, G. C. Int J Fracture 1980, 16, 499.
4. Echtermeyer, A. T.; Engh, B.; Buene, L. Composites 1995, 26, 10.
5. Song, D. Y.; Otani, N. Mater Sci Eng A 1998, 254, 200.
6. Kallrath, J.; Altstadt, V.; Schloder, J. P.; Block, H. G. Polym Test 1999, 18, 11.
7. Caprino, G.; Prisco, U.; Giorleo, L. Compos A 2007, 38, 234.
8. Petrovicova, E.; Knight, R.; Schadler, L. S.; Twardowski, T. E. J Appl Polym Sci 2000, 78, 2272.
9. Zhang, Z.; Yang, J. L.; Friedrich, K. Polymer 2004, 45, 3481.
10. Reddy, C. S.; Das, C. K.; Narkis, M. Polym Compos 2005, 26, 806.
11. Tjong, S. C.; Bao, S. P. J Polym Sci Part B: Polym Phys 2005, 43, 585.
12. Wang, Z. D.; Lu, J. J. Appl Compos Mater 2007, 14, 33.
13. Mark, J. E. Polym Eng Sci 1996, 36, 2905.
14. Wang, C. S.; Leu, T. S. Polymer 2000, 41, 3581.
15. Delozier, D. M.; Orwoll, R. A.; Cahoon, J. F.; Ladislaw, J. S.; Smith, J. G.; Connell, J. W. Polymer 2003, 44, 2231.
16. Wang, Z. D.; Lu, J. J.; Li, Y.; Fu, S. Y.; Jiang, S. Q.; Zhao, X. X. Mater Sci Eng B 2005, 123, 216.
17. Brechet, Y.; Cavaille, J. Y. Y.; Chabert, E.; Chazeau, L.; Dendievel, R.; Flandin, L.; Gauthier, C.. Adv Eng Mater 2001, 3, 571.
18. Yang, J. N.; Liu, M. D. J Compos Mater 1977, 11, 176.
19. Charewicz, A.; Daniel, I. M. ASTM STP 1986, 90, 274.
20. Poursartip, A.; Beaumont, P. W. R. Compos Sci Technol 1986, 25, 283.
21. Yang, J. N.; Lee, L. J.; Sheu, D. Y. Compos Struct 1992, 21, 91.
22. Zhao, T. S. Acta Metall Sin A: Phys Metall Mater Sci 1993, 64, 268.
23. Chankov, D. S.; Vesselinov, K. V. Int J Pres Ves Pip 1998, 75, 955.
24. Lee, C. S.; Hwang, W. Polym Compos 2000, 21, 798.
25. Hwang, W.; Lee, C. S.; Park, H. C.; Cho, I. J Adv Mater 1995, 26, 3.
26. Kawai, M. Compos A 2004, 35, 955.